Stress-Based Plaque Vulnerability Index and Assessment for Carotid Atherosclerotic Plaques Using Patient-Specific Vessel Material Properties

Qingyu Wang[1], Dalin Tang[1, 2, *], Gador Canton[3], Zheyang Wu[2],
Thomas S. Hatsukami[4], Kristen L. Billiar[5] and Chun Yuan[6]

Abstract: Cardiovascular diseases are closely linked to atherosclerotic plaque development and rupture. Assessment of plaque vulnerability is of fundamental significance to cardiovascular research and disease diagnosis, prevention, treatment and management. Magnetic resonance image (MRI) data of carotid atherosclerotic plaques from 8 patients (5 male, 3 female; age: 62-83, mean=71) were acquired at the University of Washington (UW), Seattle by the Vascular Imaging Laboratory (VIL) with written informed consent obtained. Patient-specific vessel material properties were quantified using Cine MRI data for modeling use. 3D thin-layer models were used to obtain plaque stress and strain for plaque assessment. A stress-based plaque vulnerability index (SPVI) was proposed to combine mechanical analysis, plaque morphology and composition for more complete carotid plaque vulnerability assessment. The five intervals (unit: kPa) [0, 46.8), [46.8, 80), [80, 92), [92, 103), and [103, +∞) from *in vivo* material models were used for SPVI values of 0, 1, 2, 3 and 4, respectively. The optimized agreement rate was 85.19%. The use of patient-specific material properties in plaque models could potentially improve the accuracy of model stress/strain calculations. SPVI has the potential to improve the current image-based screening and plaque vulnerability assessment schemes.

1 Introduction

Cardiovascular diseases are the major cause of death in the world [World Health

---

[1] School of Biological Science and Medical Engineering, Southeast University, Nanjing, 201196, China.

[2] Mathematical Sciences Department, Worcester Polytechnic Institute, Worcester, MA 01609, USA.

[3] Department of Mechanical Engineering, University of Washington, Seattle, WA 98195, USA.

[4] Division of Vascular Surgery, University of Washington, Seattle, WA 98195, USA.

[5] Biomedical Engineering Department, Worcester Polytechnic Institute, Worcester, MA 01609, USA.

[6] Department of Radiology, University of Washington, Seattle, WA 98195, USA.

[*] Corresponding Author: Dalin Tang. Email: dtang@wpi.edu.

Organization (2011)]. Atherosclerotic plaques may rupture without warning and cause fatal clinical events such as heart attack and stroke. It has been suggested that mechanical forces play an important role in plaque rupture process and should be considered in an integrated way with plaque morphology and composition for possible improvement of plaque assessment schemes [Tang, Kamm, Yang et al. (2014)]. Currently, patient screening and diagnosis are primarily based on clinician's experiences with the aid of medical images. Increasing evidence show that such medical imaging technologies are not enough to identify the population at risk of adverse outcome before the actual event occurs [Naghavi, Libby, Falk et al. (2003)]. It has been hypothesized that image-based plaque models of the mechanical stress and strain conditions may be useful for more accurate plaque vulnerability assessment and prediction of future adverse clinical events.

In recent years, MRI techniques have shown great potential to non-invasively quantify plaque size, shape and components (fibrous cap, lipid-rich necrotic core and calcification/inflammation) [Saam, Ferguson, Yarnykh et al. (2005)]. Yuan et al. developed multi-contrast techniques to improve the quality of MR-images and to better differentiate various components of the plaque [Yuan, Mitsumori, Beach et al. (2001); Yuan, Mitsumori, Ferguson et al. (2001)]. With the advances of medical imaging technologies [Underhill, Hatsukami, Fayad et al. (2010); Yuan, Zhang, Polissar et al. (2002); He, Wang, Huang, et al. (2016)], image-based computational models have been introduced to calculate plaque stress/strain conditions and investigate their association with plaque progression and rupture [Friedman, Krams, Chandran et al. (2010); Tang, Teng, Canton et al. (2009); Holzapfel, Stadler, Schulze-Bause et al. (2002); Bluestein, Alemu, Avrahami et al. (2008); Teng, Canton, Yuan et al. (2010); Tang, Yang, Zheng et al. (2004); Li, Howarth, Trivedi et al. (2006)]. However, the accuracy of the computational results is heavily dependent on the data and assumptions used by those models. Data needed for image-based plaque computational models include: a) Plaque morphology and components; b) Vessel and plaque component material properties; and c) Blood flow and pressure conditions [Tang, Kamm, Yang et al. (2014)]. While many image-based models used patient-specific plaque morphology data, patient-specific vessel material properties are lacking in those models [Yang, Tang, Atluri et al. (2010); Yang, Tang, Yuan et al. (2008); Yang, Canton, Yuan et al. (2010)]. Non-invasive techniques to obtain *in vivo* patient-specific vessel material properties are needed to further improve the *in vivo* image-based plaque models [Nieuwstadt, Fekkes, Hansen et al. (2015); Smoljkić, Vander Sloten, Segers et al. (2015); Liu, Canton, Yuan et al. (2012); Wang, Canton, Guo et al. (2017)]. Liu et al. introduced a non-invasive approach to quantify patient-specific vessel material properties and plaque circumferential shrinkage rate between *in vivo* and "no-load" vessel geometries [Liu, Canton, Yuan et al. (2012)]. Their material properties and circumferential shrinkage rate were calculated by 2D plaque models. Their results showed that effective Young's Modulus (YM) from the 12 human carotid arteries varied from 137 kPa to 1435 kPa and vessel circumferential shrinkage to "no-load" condition varied from 6% to 32%. Our previous work indicated that *in vivo* carotid vessel material properties have large variations from patient to patient, and vessel stiffness has an impact on stress and strain calculations. *In vivo* material plaque model shows significant difference with old material plaque model on stress and strain calculations. These differences showed that using *in vivo* material model to replace

old material model would improve the accuracy of stress and strain calculation [Wang, Canton, Guo et al. (2017)].

The foundation for plaque classifications was established by Stary et al. in a series of American Heart Association (AHA) committee reports on vascular lesions, which provided a histological lesion classification scheme [Stary, Chandler, Glagov et al. (1994); Stary, Chandler, Dinsmore et al. (1995)]. Among the AHA Type I-VIII lesions, Type I-IV are considered stable (I-III) or minimally unstable (IV). Types V (lipid-rich), VI (complex), VII (calcified), and VIII (fibrotic) are the advanced plaques capable of rupture. Using non-invasive MRI techniques, Cai et al. developed a classification system for carotid plaques based on *in vivo* MRI [Cai, Hatsukami, Ferguson et al. (2002)]. Tang et al. introduced a "local maximum stress hypothesis" to identify the critical site and stress conditions in the plaque, and proposed an ex vivo MRI-based computation plaque vulnerability index (CPVI) to determine plaque vulnerability [Teng, Canton, Yuan et al. (2010); Tang, Yang, Zheng et al. (2005); Tang, Teng, Canton et al. (2009)].

In this paper, a stress-based plaque vulnerability index (SPVI) was introduced and its value was assigned for all available slices using critical stress values from models with patient-specific material data and old material data. The resulting SPVI classifications were compared with a morphological plaque severity index (MPSI) which was defined based on plaque morphological characteristics known to correlate with plaque vulnerability [Cai, Hatsukami, Ferguson et al. (2002)].

2 Method

2.1 MRI data acquisition

Serial MRI data of carotid atherosclerotic plaques from 8 patients (5 male, 3 female; age: 62-83, mean=71) were acquired at the University of Washington (UW), Seattle by the Vascular Imaging Laboratory (VIL) using protocols approved by the UW Institutional Review Board and with written informed consent obtained. For each patient, MRI slices at baseline (Time 1, T1) and follow-up (Time 2, T2, Scan time intervals were about 18 months) were matched up using vessel bifurcation and stenosis features by experienced MR image readers. Cuff systolic and diastolic arm pressures were recorded for modeling use. *In vivo* Cine and 3D multi-contrast MR images of the carotid arteries were acquired using a 3.0T whole-body scanner (Philips Achieva, R2.6.1, Best, The Netherlands) and a dedicated 8-channel, phased array carotid coil. The carotid bifurcation was located on 2D TOF (Time of Flight) and oblique black blood MR images. A 3.5 cm region centered on the carotid bifurcation was imaged by high-resolution axial bright and black blood imaging. Detailed data acquisition and segmentation procedures were published before and are omitted here [Tang, Teng, Canton et al. (2009); Wang, Canton, Guo et al. (2017)]. For each patient, locations with Cine sequence and nearly-circular lumen cross-section were selected for calculating the material parameter values in the modified Mooney-Rivlin model [Tang, Teng, Canton et al. (2009); Wang, Canton, Guo et al. (2017)]. Fig. 1 gives 15 selected MRI slices with segmented contour plots of the plaque.
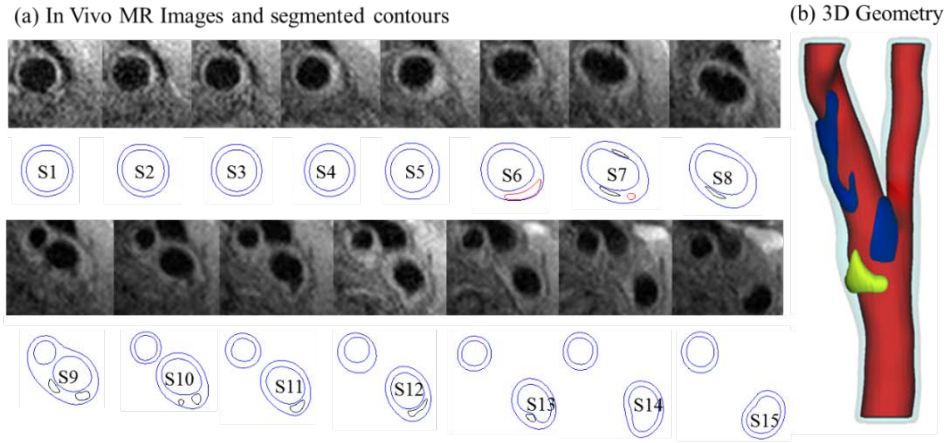
Figure 1: A plaque example showing MRI slices, segmented contours, and re-constructed geometry. (a) *In vivo* MR-images and segmented contour plots showing plaque components (Blue: lumen, vessel wall; black: calcification; red: lipid core); (b): 3D reconstructed geometry (Red: lumen; light blue: vessel; blue: calcification; yellow: lipid core)

2.2 Computational models, mesh generation and solution methods

A 3D thin-layer modeling approach introduced by Huang et al. [Huang, Yang, Zheng et al. (2016)] was used to determine material parameter values in our selected material model. For every slice that Cine data was available, a thin slice thickness (0.5 mm) was added to make a 3D thin-layer model [Wang, Canton, Guo et al. (2017)]. The carotid artery was assumed to be hyperelastic, isotropic, incompressible and homogeneous. The nonlinear modified Mooney-Rivlin (M-R) model was selected to describe the material properties of the vessel wall [Bathe (2002)]. The strain energy function was given by:

$$W = c_1(I_1 - 3) + c_2(I_2 - 3) + D_1\big[\exp\big(D_2(I_1 - 3)\big) - 1\big], \tag{1}$$

$$I_1 = \sum C_{ii}, \; I_2 = \frac{1}{2}\big[I_1{}^2 - C_{ij}C_{ij}\big], \tag{2}$$

Where $C = [C_{ij}] = X^T X$ is the right Cauchy-Green deformation tensor; I_1 and I_2 are the invariants of C. $X = [X_{ij}] = \left[\frac{\partial x_i}{\partial a_j}\right]$ is the deformation gradient. c_1, c_2, D_1 and D_2 form the material parameter set. The modified Mooney-Rivlin model was selected because it was able to fit carotid artery vessel properties measured by uniaxial and biaxial mechanical testing data and good agreement was obtained [Kural, Cai, Tang et al. (2012)]. According to our previous studies/research [Tang, Yang, Zheng et al. (2004)], material parameters c_i and D_i (i=1,2) were chosen to match experimental measurements: old vessel material/fibrous cap, c_1=36.8 kPa, D_1=14.4 kPa, D_2=2; lipid core/hemorrhage, c_1=2 kPa, D_1=2 kPa, D_2=1.5; calcification, c_1=368 kPa, D_1=144 kPa, D_2=2.0; loose matrix, c_1=18.4 kPa, D_1=7.2 kPa; D_2=1.5. c_2=0 for all materials [Tang, Yang, Zheng et al. (2004)]. And the corresponding *in vivo* material data calculation for 8 patients were published before and are omitted here [Wang, Canton, Guo et al. (2017)].

The 3D thin-layer model was solved by ADINA (Adina R&D, Watertown, MA) to obtain

mechanical conditions [Bathe (2002)]. Details about our pre-shrink-stretch model construction process and component-fitting mesh generation technique can be found in [Tang, Kamm, Yang et al. (2014)].

2.3 Definition and calculation of critical stress

It is known that thin plaque cap is closely related to plaque rupture. Thus all locations where a thin region covers a plaque component were considered as candidate critical sites. It should be noted that our "thin region" includes fibrous cap over a lipid core, as well as "cap" over calcification and other plaque components. The site with the maximum Stress (maximum principal stress) value among all the candidate sites was defined as the critical site, and the stress value at this site was defined as the critical stress [Tang, Yang, Zheng et al. (2005); Tang, Teng, Canton et al. (2009)]. For slices without any components, critical stress was defined as zero since these slices are very stable.

2.4 Assignment of morphological plaque severity index (MPSI)

Since histological data is in general not available for *in vivo* studies, a morphological plaque severity index (MPSI) was introduced (Tab. 1) and assigned to each segmented MRI slice based on plaque morphological features known to correlate with plaque vulnerability from histopathological studies [Cheng, Loree, Kamm et al. (1993); Kerwin, Xu, Liu et al. (2007); Long, Xu, Ariff et al. (2000)]. These features include: 1) The size and distribution of the soft lipid rich necrotic core (NC); 2) The fibrous cap thickness (which correlates with plaque stability); and 3) The presence of ulcer, intraplaque hemorrhage and thrombi. MPSI values (0, 1, 2, 3 to 4) indicate the level of increasing severity. The MPSI definitions are closely associated with the AHA (American Heart Association) lesion type classifications (see Tab. 1).

Table 1: Morphological plaque vulnerability index (MPSI) classifications and comparison with AHA classifications

MPSI	AHA lesion types	Description	Level of vulnerability
0	I or II	Normal or nearly normal wall.	Very stable
1	III	Moderate intimal thickening, no extracellular lipid, calcification or significant inflammation.	Stable
2	IV/V with≤30% NC; or VII; or VIII	Advanced lesion with small necrotic core, or can be fibrotic or calcified, fibrous cap (>200 μm).	Slightly unstable
3	IV/V with 30-40% NC	Advanced lesion with Moderate lipid core and fibrous cap (150-200 μm).	Moderately unstable
4	IV/V (with>40% NC; or VI)	Advanced lesion with a very large necrotic core, thin fibrous cap (<150 μm), or with fibrous cap rupture, ulceration, or intraplaque hemorrhage.	Very unstable

2.5 SPVI assignment and data analysis

Each slice was assigned a SPVI value (0, 1, 2, 3 or 4) according to its critical stress by using five stress intervals, which were determined to have best match rate with MPSI. Correlations between SPVI values and plaque morphological features including lipid core size, cap thickness and normalized wall index were analyzed. Average stress/strain and critical stress/strain on the lumen and all the cap nodes covering the lipid-rich pool were recorded for comparison. To be clear, since stress and strain are tensors, maximum principal stress and maximum principal strain were used as the scalar representatives of stress and strain to present our results. Fig. 2 presents 5 representative slices with above described morphological characteristics. Correlation studies were performed using standard student *t*-test method.

(a) In Vivo MRI images of selected plaques with different classifications.
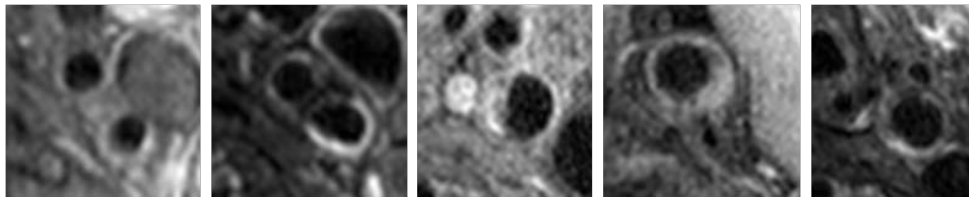
(b) Segmented contours (Black: calcification; Red: Lipid core);

| MPSI=0 | MPSI=1 | MPSI=2 | MPSI=3 | MPSI=4 |
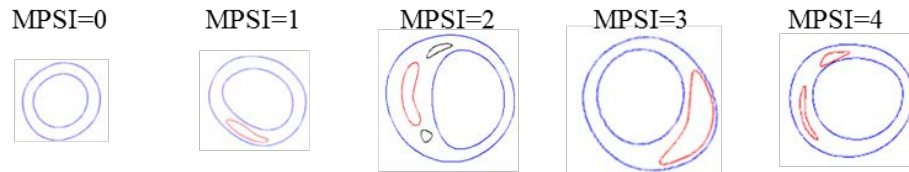
(c) Critical Site and Critical Stress (kPa) on Stress Band Plot

| SPVI=0 | SPVI=1 | SPVI=2 | SPVI=3 | SPVI=4 |

| C-Stress = 40.2kPa | C-Stress = 70.68kPa | C-Stress = 84.41kPa | C-Stress = 100.1kPa | C-Stress = 153.8kPa |

(d) SPVI intervals (kPa)

| [0, 46.8) | [46.8, 80) | [80, 92) | [92, 103) | [103, +∞) |
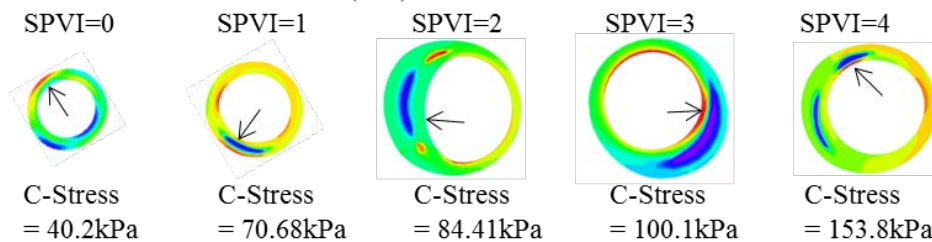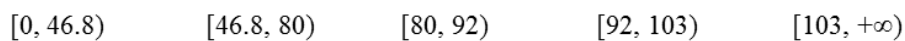
Figure 2: Plaque samples showing morphological features and critical stress values for plaque classifications. (a) *In vivo* MR-images; (b) segmented contour plots showing plaque components (Black: calcification; Red: Lipid core); (c) stress plots showing critical stress of corresponding slices; (d) *In vivo* SPVI intervals were calculated based on critical stress values at critical sites

3 Results

3.1 Five stress intervals values for SPVI using in vivo material and old material

Figs. 2(b) and 2(c) give an example for the MPSI and SPVI groups, respectively. Figs. 3 and 4 show the scattered plot for critical stress from *in vivo* material models and old material model. A simple numerical code was used to determine five stress intervals [0, a), [a, b), [b, c), [c, d), and [d, +∞) corresponding to SPVI values 0-4 to reach the best agreement between SPVI and MPSI. The five stress intervals for the *in vivo* material models were (unit: kPa) [0, 46.8), [46.8, 80), [80, 92), [92, 103), and [103, +∞) corresponding to SPVI values of 0, 1, 2, 3 and 4, respectively. The five intervals for the old material models were [0, 50.4), [50.4, 82), [82, 91), [91, 146.5), and [146.5, +∞) for SPVI values of 0, 1, 2, 3 and 4.

One important value the research community would like to have is a threshold stress value one could use to claim that a plaque is highly vulnerable. According to the SPVI stress intervals, the threshold critical stress value for a plaque to be considered highly unstable (SPVI=4) is 103 kPa from *in vivo* material models. The threshold stress value became 146.5 kPa using old material models.
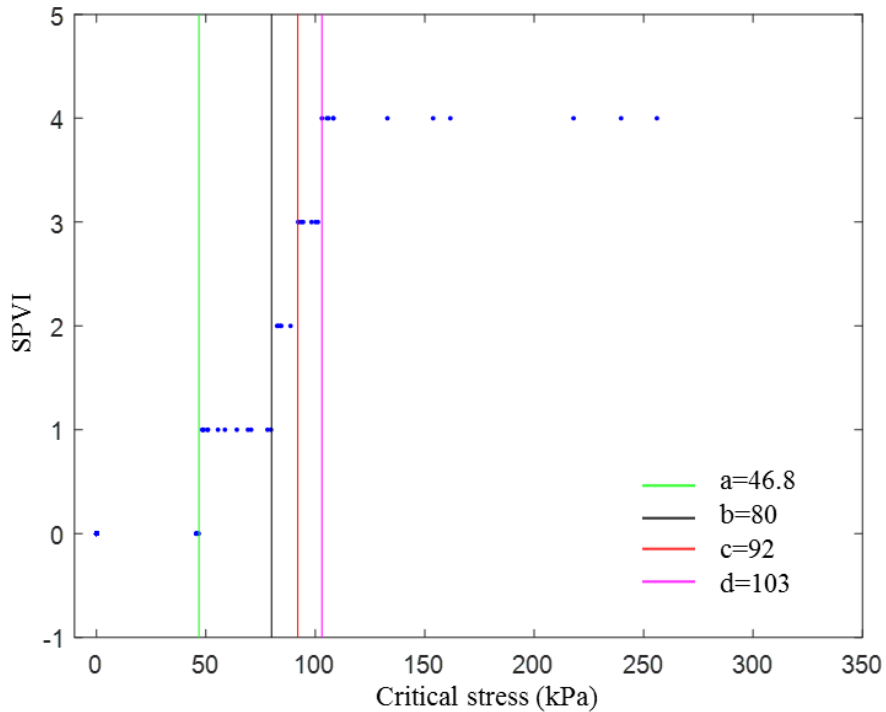
Figure 3: Scattered plot for critical stress from *in vivo* material model and five stress intervals [0, a), [a, b), [b, c), [c, d), and [d, +∞) corresponding to SPVI group values 0-4 to reach the best agreement between SPVI and MPSI
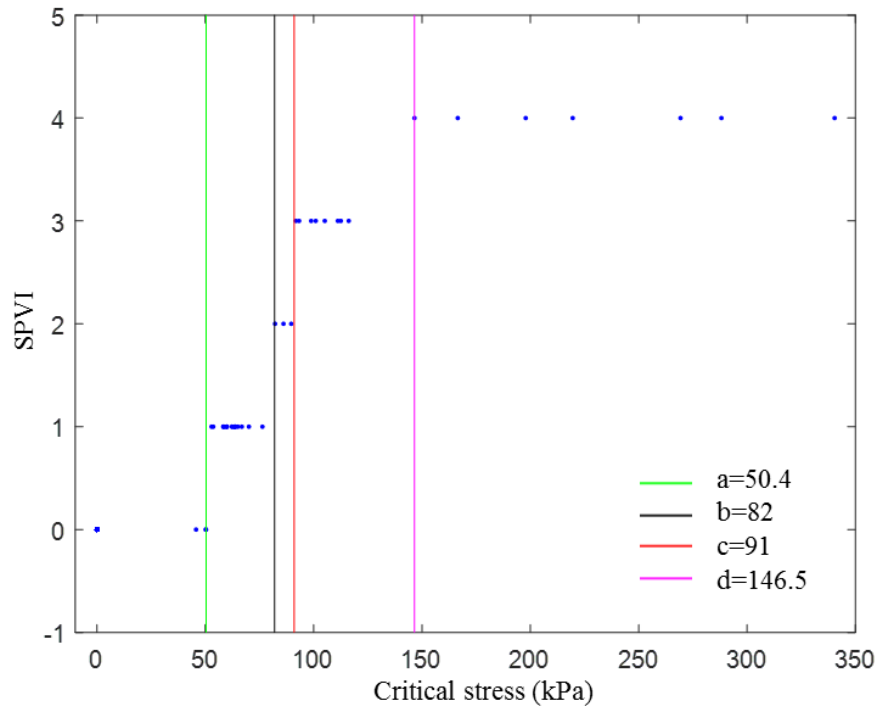
Figure 4: Scattered plot for critical stress from old material model and five stress intervals [0, a), [a, b), [b, c), [c, d), and [d, +∞) corresponding to SPVI group values 0-4 to reach the best agreement between SPVI and MPSI

3.2 Agreement rate between MPSI and SPVI using in vivo and old material models.

Tab. 2 and Tab. 3 lists number of cases and agreement rate for each SPVI grade group. The optimized agreement rate from *in vivo* material models and old material models was 85.19% and 83.95%, respectively. The Pearson correlation coefficient between SPVI and MPSI was 0.9103 ($p<0.0001$) and 0.8661 ($p<0.0001$), respectively. The ones with MPSI being 3 have the lowest match rates, which are 57.14% and 42.86%, respectively. From the agreement rates, all of the *in vivo* results more than 50%. For the high risk plaque Groups 3 and 4, *in vivo* SPVI values shows better agreement with MPSI than old SPVI values.

Table 2: Case distributions according to MPSI and agreement rate between MPSI and SPVI using *in vivo* material models

Group	0	1	2	3	4	Total
MPSI slice	44	15	5	7	10	81
SPVI slice (*in vivo*)	46	13	5	6	11	81
Matched slice	44	11	3	4	7	69
Agreement rate (%)	100.0	73.33	60.00	57.14	70.00	85.19
Agreement rate=(Matched slice/MPSI slice)×100%						

Table 3: Case distributions according to MPSI and agreement rate between MPSI and SPVI using old material models

Group	0	1	2	3	4	Total
MPSI slice	44	15	5	7	10	81
SPVI slice (old)	45	18	3	8	7	81
Matched slice	44	12	3	3	6	68
Agreement rate (%)	100.0	80.00	60.00	42.86	60.00	83.95
Agreement rate=(Matched slice/MPSI slice)×100%						

3.3 Impact of patient-specific material properties on SPVI

Tab. 4 lists the SPVI change rate for slices using old material models compared to using *in vivo* material models. The changed slices for SPVI using old material models compared to using *in vivo* material models were listed in Tab. 4. The total change rate was 18.52%. The ones with SPVI being 4 have the highest change rates, which was 54.55%. It shows using patient-specific material properties in computational models would lead to significant improvement on plaque vulnerability assessment. SPVI is sensitive to the material of computational models.

Table 4: The variation of SPVI between *in vivo* material models and old material models

Group	0	1	2	3	4	Total
In vivo SPVI slice	46	13	5	6	11	81
Changed slice	2	2	3	2	6	15
Changed rate (%)	4.30	15.38	60.00	33.33	54.55	18.52
Changed rate=(Changed slice/*In vivo* SPVI slice)×100%						

4 Discussion

4.1 Significance of in vivo patient-specific vessel material properties on plaque Vulnerability predictions

Using the old material models had 47.06% changed rate for unstable plaque level (SPVI value 3 and 4). Considering that most research reports used the old material model. Our results indicated that plaque vulnerability predictions should use *in vivo* vessel material properties when it becomes available.

4.2 Threshold critical stress value for highly vulnerable plaques

It should be noted that our threshold critical stress value from *in vivo* material model are lower than the value from old material model (103 kPa and 146.5 kPa for SPVI=4) for several reasons: a) Our models were based on *in vivo* material models could led to different stress predictions; b) Our 81 slices from 16 plaque samples included cases from stable to unstable and the number of MPSI=4 were only 10 slices.

4.3 Purpose of introducing SPVI and modeling considerations

The purpose of introducing SPVI is to have a more complete plaque assessment scheme

which includes mechanical factors, plaque morphological features and tissue compositions for possible patient-screening applications. Results from 81 slices suggested that SPVI and MPSI had good agreement on plaque classifications. At the same time, the disagreement cases suggested that SPVI scheme may complement image-only assessment schemes and lead to potential improvements. The present study is the first *in vivo* case study quantifying differences between mechanics-image combined and morphology-only assessment schemes.

It should be understood that plaque rupture is a multi-faceted process. SPVI covers only mechanical and morphological factors. We hope SPVI could provide complementing information for plaque assessment that image alone could not provide.

4.4 Model limitations

Cine MRI was used to determine vessel material parameter values, matching *in vivo* plaque geometries under both systolic and diastolic pressure conditions. Multi-layer structure and anisotropic material properties of arteries were not considered since MRI does not provide layer information. Another limitation was that location-specific pressure measurement was not available. Noninvasive acquisition of intra-plaque pressure data remains a challenge. Furthermore, larger patient size will potentially lead to better plaque vulnerability prediction result.

5 Conclusions

Our preliminary results indicated that *in vivo* carotid vessel material properties have large variations from patient to patient, and vessel stiffness has an impact on plaque assessment. *In vivo* material plaque model shows significant difference with old material plaque model on SPVI calculations. These differences showed that using *in vivo* material model to replace old material model would improve the accuracy of plaque assessment.

References

Bathe, K. J. (2002): *Theory and Modeling Guide*. Vol I & II: ADINA and ADINA-F, ADINA R & D, Inc., Watertown, MA.

Bluestein, D.; Alemu, Y.; Avrahami, I.; Gharib, M.; Dumont, K. et al. (2008): Influence of microcalcifications on vulnerable plaque mechanics using FSI modeling. *Journal of Biomechanics*, vol. 41, no. 5, pp. 1111-1118.

Cai, J. M.; Hatsukami, T. S.; Ferguson, M. S.; Small, R.; Polissar, N. L. et al. (2002): Classification of human carotid atherosclerotic lesions with *in vivo* multicontrast magnetic resonance imaging. *Circulation*, vol. 106, pp. 1368-1373.

Cheng, G. C.; Loree, H. M.; Kamm, R. D.; Fishbein, M. C.; Lee, R. T. (1993): Distribution of circumferential stress in ruptured and stable atherosclerotic lesions, a structural analysis with histopathological correlation. *Circulation*, vol. 87, pp. 1179-1187.

Friedman, M. H.; Krams, R.; Chandran, K. B. (2010): Flow interactions with cells and tissues: Cardiovascular flows and fluid-structure interactions. *Annals of Biomedical Engineering*, vol. 38, no. 3, pp. 1178-1187.

He, C. L.; Wang, J. Q.; Huang, Y. X.; Zhu, T. J.; Miao, Y. H. et al. (2016): The correlation between texture features and fibrous cap thickness of lipid-rich atheroma based on optical coherence tomography imaging. *Molecular & Cellular Biomechanics*, vol. 13, no. 1, pp. 23-36.

Holzapfel, G. A.; Stadler, M.; Schulze-Bause, C. A. (2002): A layer-specific three dimensional model for the simulation of balloon angioplasty using magnetic resonance imaging and mechanical testing. *Annals of Biomedical Engineering*, vol.30, no. 6, pp. 753-767.

Huang, X.; Yang, C.; Zheng, J.; Bach, R.; Muccigrosso, D. et al. (2016): 3D MRI-based multicomponent thin layer structure only plaque models for atherosclerotic plaques. *Journal of Biomechanics*, vol. 49, no. 13, pp. 2726-2733.

Kerwin, W.; Xu, D.; Liu, F.; Saam, T.; Underhill, H. et al. (2007): Magnetic resonance imaging of carotid atherosclerosis: Plaque analysis. *Topics in Magnetic Resonance Imaging*, vol. 18, pp. 371-378.

Kural, M. H.; Cai, M.; Tang, D.; Gwyther, T.; Zheng, J. et al. (2012): Planar biaxial characterization of diseased human coronary and carotid arteries for computational modeling. *Journal of Biomechanics*, vol. 45, no. 5, pp.790-798.

Li, Z. Y.; Howarth, S.; Trivedi, R. A.; U-King-Im, J. M.; Graves, M. J. et al. (2006): Stress analysis of carotid plaque rupture based on *in vivo* high resolution MRI. *Journal of Biomechanics*, vol. 39, no. 14, pp. 2611-2622.

Liu, H.; Canton, G.; Yuan, C.; Yang, C.; Billiar, K. et al. (2012): Using *in vivo* cine and 3D multi-contrast MRI to determine human atherosclerotic carotid artery material properties and circumferential shrinkage rate and their impact on stress/strain predictions. *Journal of Biomechanical Engineering*, vol. 134, no. 1, pp. 223-233.

Long, Q.; Xu, X. Y.; Ariff, B.; Thom, S. A.; Hughes, A. D. et al. (2000): Reconstruction of blood flow patterns in a human carotid bifurcation: A combined CFD and MRI study. *Journal of Magnetic Resonance Imaging*, vol. 11, pp. 299-311.

Naghavi, M.; Libby, P.; Falk, E.; Casscells, S. W.; Litovsky, S. et al. (2003): From vulnerable plaque to vulnerable patient: A call for new definitions and risk assessment strategies: Part I. *Circulation*, vol. 108, no. 14, pp. 1664-1672.

Nieuwstadt, H. A.; Fekkes, S.; Hansen, H. H.; de Korte, C. L.; van der Lugt, A. et al. (2015): Carotid plaque elasticity estimation using ultrasound elastography, MRI, and inverse FEA-A numerical feasibility study. *Medical Engineering & Physics*, vol. 37, no. 8, pp. 801-807.

Saam, T.; Ferguson, M. S.; Yarnykh, V. L.; Takaya, N.; Xu, D. et al. (2005): Quantitative evaluation of carotid plaque composition by *in vivo* MRI. *Arteriosclerosis, Thrombosis, and Vascular Biology*, vol. 25 no. 1, pp. 234-239.

Smoljkić, M.; Vander Sloten, J.; Segers, P.; Famaey, N. (2015): Non-invasive, energy-based assessment of patient-specific material properties of arterial tissue. *Biomech Model Mechanobiol*, vol. 14, no. 5, pp. 1045-1056.

Stary, H. C.; Chandler, A. B.; Glagov, S.; Guyton, J. R.; Insull, Jr. W. et al. (1994): A definition of initial, fatty streak and intermediate lesions of atherosclerosis. A report from the Committee on Vascular Lesions of the Council on Arteriosclerosis, AHA. *Circulation*, vol. 89, pp. 2462-2478.

Stary, H. C.; Chandler, A. B.; Dinsmore, M. D.; Fuster, V.; Glagov, S. et al. (1995): Definitions of advanced types of atherosclerotic lesions and the histological classification of atherosclerosis. A report from the Committee on Vascular Lesions of the Council on Arteriosclerosis, AHA. *Circulation*, vol. 92, pp. 1355-1374.

Tang, D.; Yang, C.; Zheng, J.; Woodard, P. K.; Sicard, G. A. et al. (2004): 3D MRI-based multi-component FSI models for atherosclerotic plaques: A 3-D FSI model. *Annals of Biomedical Engineering*, vol. 32, no. 7, pp. 947-960.

Tang, D.; Yang, C.; Zheng, J.; Woodard, P. K.; Saffitz, J. E. et al. (2005): Local maximal stress hypothesis and computational plaque vulnerability index for atherosclerotic plaque assessment. *Annals of Biomed Engineering*, vol. 33, no. 12, pp. 1789-1801.

Tang, D.; Teng, Z.; Canton, G.; Hatsukami, T. S.; Dong, L. et al. (2009): Local critical stress correlates better than global maximum stress with plaque morphological features linked to atherosclerotic plaque vulnerability: An *in vivo* multi-patient study. *BioMedical Engineering OnLine*, vol. 8, no. 1, pp. 15.

Tang, D.; Teng, Z.; Canton, G.; Yang, C.; Ferguson, M. et al. (2009): Sites of rupture in human atherosclerotic carotid plaques are associated with high structural stresses: An *in vivo* MRI-based 3D fluid-structure interaction study. *Stroke*, vol. 40, pp. 3258-3263.

Tang, D.; Kamm, R. D.; Yang, C.; Zheng, J.; Canton, G. et al. (2014): Image-based modeling for better understanding and assessment of atherosclerotic plaque progression and vulnerability: Data, modeling, validation, uncertainty and predictions. *Journal of Biomechanics*, vol. 47, no. 4, pp. 834-846.

Teng, Z.; Canton, G.; Yuan, C.; Ferguson, M.; Yang, C. et al. (2010): 3D critical plaque wall stress is a better predictor of carotid plaque rupture sites than flow shear stress: an *in vivo* MRI-based 3D FSI study. *Journal of Biomechanical Engineering*, vol. 132, no. 3.

Underhill, H. R.; Hatsukami, T. S.; Fayad, Z. A.; Fuster, V.; Yuan, C. (2010): MRI of carotid atherosclerosis: Clinical implications and future directions. *Nature Reviews Cardiology*, vol. 7, no. 3, pp. 165-173.

Wang, Q. Y.; Canton, G.; Guo, J.; Guo, X.; Hatsukami, T. S. et al. (2017): MRI-based patient-specific human carotid atherosclerotic vessel material property variations in patients, vessel location and long-term follow up. *Plos One*, vol. 12, no. 7.

World Health Organization. (2011): *Global Atlas on Cardiovascular Disease*

Prevention and Control. Geneva: World Health Organization.

Yang, C.; Tang, D.; Yuan, C.; Kerwin, W.; Liu, F. et al. (2008): Meshless generalized finite difference method and human carotid atherosclerotic plaque progression simulation using multi-year MRI patient-tracking data. *Computer Modeling in Engineering & Sciences*, vol. 28, no. 2, pp. 95-107.

Yang, C.; Canton, G.; Yuan, C.; Ferguson, M.; Hatsukami, T. S. et al. (2010): Advanced human carotid plaque progression correlates positively with flow shear stress using follow-up scan data: An *in vivo* MRI multi-patient 3D FSI study. *Journal of Biomechanics*, vol. 43, no. 13, pp. 2530-2538.

Yang, C.; Tang, D.; Atluri, S. (2010): Three-dimensional carotid plaque progression simulation using meshless generalized finite difference method based on multi-year MRI patient-tracking data. *Computer Modeling in Engineering & Sciences*, vol. 57, no. 1, pp. 51-76.

Yuan, C.; Mitsumori, L. M.; Beach, K. W.; Maravilla, K. R. (2001): Special review: Carotid atherosclerotic plaque: Noninvasive MR characterization and identification of vulnerable lesions. *Radiology*, vol. 221, pp. 285-299.

Yuan, C.; Mitsumori, L. M.; Ferguson, M. S.; Polissar, N. L.; Echelard, D. E. et al. (2001): *In vivo* accuracy of multispectral MR imaging for identifying lipid-rich necrotic cores and intraplaque hemorrhage in advanced human carotid plaques. *Circulation*, vol. 104, pp. 2051-2056.

Yuan, C.; Zhang, S. X.; Polissar, N. L.; Echelard, D.; Ortiz, G. et al. (2002): Identification of fibrous cap rupture with MRI is highly associated with recent transient ischemic attack or stroke. *Circulation*, vol. 105, pp. 181-185.